Probing the Lipid Membrane Dipole Potential by Atomic Force Microscopy

Yi Yang,* Kathryn M. Mayer,* Nissanka S. Wickremasinghe,* and Jason H. Hafner*†
*Department of Physics & Astronomy, and †Department of Chemistry, Rice University, Houston, Texas

ABSTRACT The electrostatic properties of biological membranes can be described by three parameters: the transmembrane potential, the membrane surface potential, and the membrane dipole potential. The first two are well characterized in terms of their magnitudes and biological effects. The dipole potential, however, is not well characterized. Various methods to measure the membrane dipole potential indirectly yield different values, and there is not even agreement on the source of the membrane dipole moment. This ambiguity impedes investigations into the biological effects of the membrane dipole moment, which should be substantial considering the large interfacial fields with which it is associated. Electrostatic analysis of phosphatidylcholine lipid membranes with the atomic force microscope reveals a repulsive force between the negatively charged probe tips and the zwitterionic lipids. This unexpected interaction has been analyzed quantitatively to reveal that the repulsion is due to a weak external field created by the internal membrane dipole potential. The analysis yields a dipole moment of 1.5 Debye per lipid with a dipole potential of +275 mV for supported phosphatidylcholine membranes. This new ability to quantitatively measure the membrane dipole moment in a noninvasive manner with nanometer scale spatial resolution will be useful in identifying the biological effects of the dipole potential.

INTRODUCTION

Biological membranes create a complex and highly anisotropic electrostatic environment that supports biological function. Electrostatic interactions in and near the membrane are typically characterized by three potentials, illustrated in Fig. 1 *A*. The transmembrane potential (ψ_{tr}) is the well-known driving force for ion transport through channels in cell membranes, a fundamental step in cell signaling and other biological processes (1). The surface potential (ψ_s) regulates the interaction of cytosolic and environmental factors with cell membranes (2). These two membrane potentials are well characterized and have clear effects on membrane function. A third membrane potential exists, however, that is rather enigmatic. The dipole potential (ψ_d) is a relatively large positive potential barrier at the membrane midplane created by inward-pointing molecular dipoles at the interfacial planes (3). Although the dipole potential has been studied for decades, it is among the least understood aspects of biological membranes. There is currently no definitive agreement on the magnitude of the dipole potential barrier, or even the source of the molecular dipole density. Considering the large interfacial fields associated with the dipole potential and the likely effect of those fields on membrane protein structure and function, an accurate characterization of the dipole potential is warranted.

A direct measurement of the dipole potential with electrodes is not currently possible since the entire effect occurs within the membrane, but there are several existing indirect methods for its measurement. Hydrophobic ions with similar chemical structures, yet opposite charge, diffuse across the membrane at significantly different rates (4). This was the initial observation that led to the concept of an internal dipole potential barrier (5). The measured transport properties of such ions can be modeled to estimate a membrane dipole potential of 150–350 mV, depending on the constituent lipid species (6,7). Alternatively, the dipole potential can be inferred from the potential difference across a lipid monolayer at an air-water interface, which yields values of 400–600 mV (8). Molecular dynamics simulations of lipid membranes can be analyzed to calculate the total electrostatic potential throughout the membrane. This method yields dipole potential values ranging from 600 to 1000 mV (9). A ratiometric fluorescence signal from di-8-ANEPPS, a voltage sensitive dye, has been shown to be proportional to the dipole potential (10), and other dyes have been developed for this purpose as well (11). While dyes are the most attractive means to study membrane dipoles in dynamic systems such as living cells, their response must be calibrated by other techniques. Therefore, this method does not represent a direct measurement of the dipole potential. Recently, the contrast of cryo-electron micrographs of lipid membrane vesicles was analyzed to measure the dipole potential, yielding a value similar to monolayer measurements (12).

We have recently demonstrated that the atomic force microscope (AFM) is a powerful tool for the analysis of membrane electrostatics (13). Due to its high force sensitivity, the AFM can probe interfacial electrostatics in a non-contact manner for minimum perturbation of the sample. Due to the sharpness of the probe, electrostatic parameters are mapped across the surface with nanometer-scale spatial resolution (14). If the data are analyzed with a numerical simulation of the nonlinear Poisson-Boltzmann equation and all parameters are characterized, the AFM yields quantitative membrane surface potentials with no adjustable parameters.

Submitted May 1, 2008, and accepted for publication August 13, 2008.

Address reprint requests to Jason Hafner, Tel.: 713-348-3205; E-mail: hafner@rice.edu.

Editor: Stuart M. Lindsay.

© 2008 by the Biophysical Society
0006-3495/08/12/5193/07 $2.00

doi: 10.1529/biophysj.108.136507

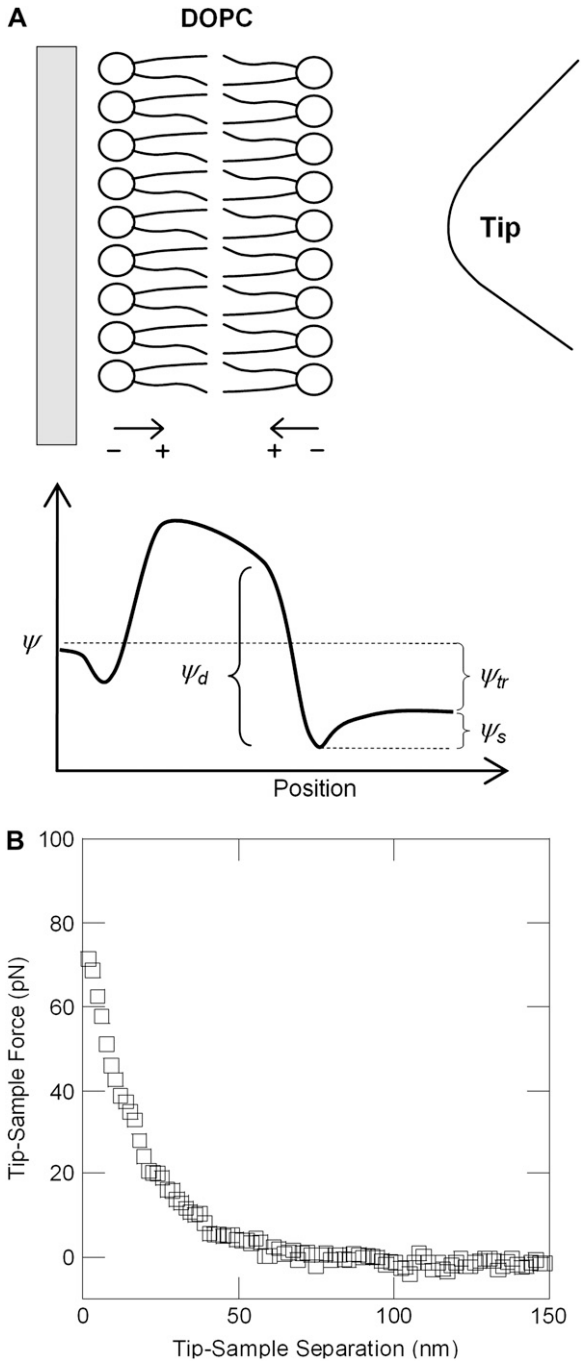

FIGURE 1 AFM analysis of the membrane dipole potential. (*A*) A schematic of the tip-sample region (not to scale), along with a plot that illustrates the three membrane potentials. (*B*) The observed repulsive force interaction between the negatively charged silicon nitride tip and DOPC membrane.

The above points were demonstrated on charged membranes created by mixing anionic and cationic lipids with zwitterionic phosphatidylcholine. However, when pure zwitterionic membranes were analyzed with a negatively charged silicon nitride tip, a repulsive force was observed as though the zwitterionic membrane were negatively charged, as seen in Fig. 1 *B*. In this article, the repulsive interaction is shown to be due to a weak external field created by the internal membrane dipole potential, thus providing a noninvasive and quantitative method for its measurement.

MATERIALS AND METHODS

Preparation of supported lipid membranes

Lyophilized dioleoylphosphatidylcholine (DOPC, Avanti Polar Lipids, Alabaster, AL) was dissolved in chloroform, dried under nitrogen gas, further dried under low vacuum for 1 h, and then hydrated with deionized water to a final lipid concentration of 2 mg/mL. Alternatively, DOPC and di-8-ANEPPS were first mixed at a 1:600 molar ratio in chloroform, and then dried and redissolved by the same procedure. The lipid solutions stood overnight in a dark, room-temperature environment followed by vigorous agitation for 1 h. The resulting multilamellar vesicle solutions were refrigerated and stored for up to two weeks. Supported lipid bilayers for AFM analysis were formed on mica substrates by vesicle fusion. A 100-μL drop of the multilamellar vesicle solution at a lipid concentration of 20–200 μg/mL (diluted from stock in deionized water) was placed on a substrate for 20 min at 35–40°C. The mica substrates were then rinsed with deionized water and placed in the AFM fluid cell in electrolyte solution for imaging in fluid tapping mode and force spectroscopy (Multimode NanoScope IV, Veeco Metrology, Santa Barbara, CA).

Force curve acquisition

All AFM experiments were carried out with silicon nitride probes (DNP, cantilever C, Veeco Probes, Santa Barbara, CA). Both tip and sample were immersed in 0.1–1 mM sodium chloride solution throughout the experiment. To record force curves over lipids, the AFM tip was situated over a lipid membrane by first imaging the topography and then positioning the tip over the lipid region. For tip charge density calibration, force curves were recorded over the silicon nitride chip of a probe from the same wafer as the tip. The gold coating on this chip was first etched with Aqua regia to reduce interference from the reflected AFM laser beam. Force curves were recorded with the Nanoscope software (Ver. 5.30r1) with 4098 data points over an 800-nm scan range at 3.49 Hz, with tip retraction triggered for a maximum cantilever deflection corresponding to ~5 nN. The force curves were processed and averaged exactly as described previously (13).

Tip radius and spring constant measurement

The radius of each individual AFM tip was measured from scanning electron microscope images. The cantilevers employed have a nominal spring constant $k = 0.32$ N/m. For improved accuracy, the spring constant of each tip was directly measured by the added mass method (15). Briefly, the thermal resonance frequency of the cantilever was measured before and after the addition of a known mass, M, by micromanipulation, yielding frequencies ν_1 and ν_2, respectively. The known mass was a 6-μm spherical silica bead with a well-defined shape and density (Bangs Laboratories, Fishers, IN). The shift in resonant frequency yields the spring constant using the following relation:

$$k = (2\pi)^2 \frac{M_1}{\left(\frac{1}{\nu_2^2}\right) - \left(\frac{1}{\nu_1^2}\right)}. \quad (1)$$

Measured values for the cantilever spring constants ranged from 0.22 to 0.30 N/m.

Electrostatic analysis

Force curves were analyzed with numerical solutions to the full nonlinear Poisson-Boltzmann equation using a commercial software package

(FlexPDE 5.0.8; PDE Solutions, Antioch, CA). For calibration of the tip charge density, the simulation was carried out for a hemispherical silicon nitride tip against a flat silicon nitride surface in electrolyte. In the electrolyte the Poisson-Boltzmann equation

$$\nabla^2\psi = \frac{2n_0e}{\varepsilon_{\text{electrolyte}}\varepsilon_0}\sinh(e\psi/k_BT), \tag{2}$$

where ψ is electrostatic potential, n_0 is the monovalent electrolyte ion density, e is the electron charge, k_B is the Boltzmann constant, and $\varepsilon_{\text{electrolyte}}$ is the dielectric constant, was solved. In the silicon nitride regions, the Laplace equation

$$\nabla\cdot(\varepsilon_o\varepsilon_{Si_3N_4}\nabla\psi) = 0 \tag{3}$$

was solved. Constant field boundary conditions were applied (16) to define the charge densities on the sample and tip,

$$\begin{aligned}\psi_1 &= \psi_2\\ (\varepsilon_1\nabla\psi_1 - \varepsilon_2\nabla\psi_2)\cdot\mathbf{n} &= \sigma/\varepsilon_o,\end{aligned} \tag{4}$$

where $\mathbf{n}$ represents the surface normal direction (17). The resulting surface potentials are converted to forces using the total stress tensor, which includes both osmotic pressure and Maxwell stress terms. Details were described previously (13). The tip-sample separation was then altered in the simulation to generate simulated force curves. The identical surface and tip charge densities were manually adjusted to make the simulated force curves match those from the experiments. In this way, an identical reference surface can be used to quantitatively measure the tip charge density.

To analyze the force curves over zwitterionic lipid membranes with a dipole model, a simulation was set up as shown in Fig. 3. Equation 2 was solved in the electrolyte regions ($\varepsilon = 80$), and Eq. 3 was solved in the silicon nitride ($\varepsilon = 6$) and mica ($\varepsilon = 6$), regions. The charged planes were given a set separation and equal charge density magnitudes. Equation 2 was solved between the charged planes ($\varepsilon = 2.2$). The above procedure was carried out to generate force curves. The force curves were fit to experimental data by adjusting the charge density magnitude on the planes. The resulting charge density magnitudes and charge plane separations yield the dipole moment per unit area reported in Fig. 4.

Fluorescence microscopy

The supported lipid membranes were imaged on an Axiovert 200 MAT microscope with an XBO 75 xenon lamp (Carl Zeiss, Jena, Germany). The excitation was filtered by 40 nm bandpass filters chosen at the red and blue edges of the di-8-ANEPPS excitation profile: 425 nm and 510 nm. The emission was observed through a 50-nm bandpass filter centered at 675 nm with a dichroic mirror at 565 nm. All filters and beam splitters were purchased from Chroma (Rockingham, VT). The images were recorded with a PhotonMax 512B CCD camera (Princeton Instruments, Princeton, NJ) at 10-s integration times. Images were recorded at each excitation wavelength, the backgrounds were subtracted from a nonfluorescent region, and the intensities were corrected for the relative efficiencies of the two excitation filters. The ratio image was then formed as the direct ratio of these processed images (425:510 nm).

RESULTS AND DISCUSSION

A possible explanation for the observed repulsive interaction shown in Fig. 1 *B* is that the zwitterionic membrane attains a negative surface charge due to counterion binding. For example, if Cl^- in the electrolyte were to form a Stern layer and neutralize some of the cationic cholines in the lipid headgroups, a net negative surface charge would remain. To test this hypothesis, force curves over zwitterionic DOPC were recorded at 0.1–1.0 mM NaCl and analyzed as described previously (13) to yield an effective surface charge density of ~ -0.004 C/m^2 with no significant dependence on salt concentration (Fig. 2). The predicted surface charge density σ due to counterion binding can be calculated from the Gouy-Chapman-Stern (GCS) model of membrane electrostatics by combining the Grahame equation,

$$\sigma = \sqrt{8\varepsilon\varepsilon_0k_BTn_0}\sinh(e\psi/2k_BT), \tag{5}$$

and the Langmuir isotherm,

$$\sigma = \sigma_{\max}\frac{KC_0e^{-ze\psi/k_BT}}{KC_0e^{-ze\psi/k_BT}+1}, \tag{6}$$

where n_0 is the Cl^- ion density far from the surface and C_0 is the corresponding concentration, ψ is the surface potential, $\sigma_{\max}$ is the maximum charge density assuming one charge per lipid, K is the binding constant of Cl^- ion to the membrane surface, and z is the valency of the Cl^- ion (18). By solving each for the surface potential and equating these two expressions, one can obtain a model for the surface charge density as a function of Cl^- ion concentration. Using literature values for the binding of the Cl^- ion to the phosphatidylcholine headgroup (19), the GCS model predicts a surface charge density of only -0.0002 C/m^2 at 1 mM electrolyte. Even arbitrarily increasing the binding constant used in the model by a factor of 10 does not raise the predicted surface charge density to the observed values. Furthermore, recent simulations suggest that the Na^+ cation will bind the lipid headgroup more strongly, resulting in a positively charged membrane rather than a negatively charged one (20). Therefore, while a Stern layer may contribute to the surface electrostatics of zwitterionic membranes, it is not sufficient to account for the data in Fig. 1 *B*.

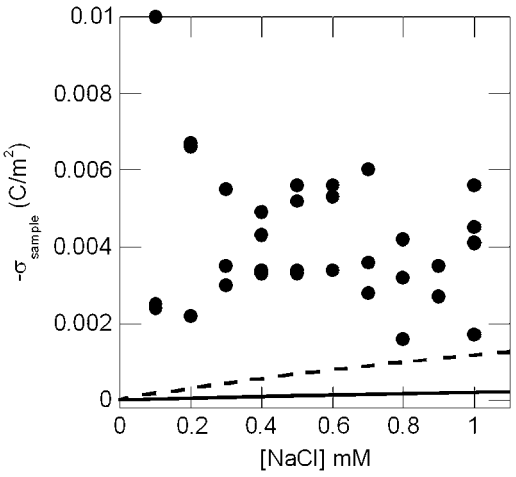

FIGURE 2 Repulsive force data measured between a silicon nitride tip and supported DOPC membranes were analyzed by a numerical model to yield an effective membrane surface charge density (*circles*). The measurements are taken from many experiments and multiple tips. GCS models of lipid membranes are shown for Cl^- binding constants of $K = 0.9$ M^{-1} (*solid line*) and $K = 10$ M^{-1} (*dashed line*).

Here we propose that the repulsive interaction is due to an external vestige of the large internal electrostatic fields associated with the dipole potential. Belaya et al. (21) calculated the external electrostatic potential of a soft interfacial plane which contains both charge and dipole densities. They found that such an interface creates a decaying external potential equivalent to that of a simple charged interface with an effective charge density. Their calculations showed that this effective charge density depends on the actual charge density and the dipole density at the interface. These results were obtained analytically by solving the linearized Poisson-Boltzmann equation while describing the charge density and dipole density with δ-functions rather than treating them as boundary conditions. Since we previously found that accurate quantitative analysis of AFM data requires the use of the nonlinear Poisson-Boltzmann equation (13), a numerical approach analogous to the analytical method of Belaya et al. was employed to analyze force data such as that in Fig. 1 *B*. A schematic of the numerical simulation is presented in Fig. 3 *A*. Two pairs of oppositely charged planes were defined at the interfacial regions between an aqueous phase and a hydrophobic interior to simulate the interfacial dipole density. The charged, supporting mica substrate was also included in the simulations (22). These dipolar charge planes represent the net effect of the various possible molecular contributions to the membrane dipole density, such as trapped water molecules, the polar headgroups, or the ester linkages of the phospholipids (3). Two charge plane separations were tested: 2 Å and 5 Å. The tip radius was characterized by electron microscopy and its charge density was characterized by force

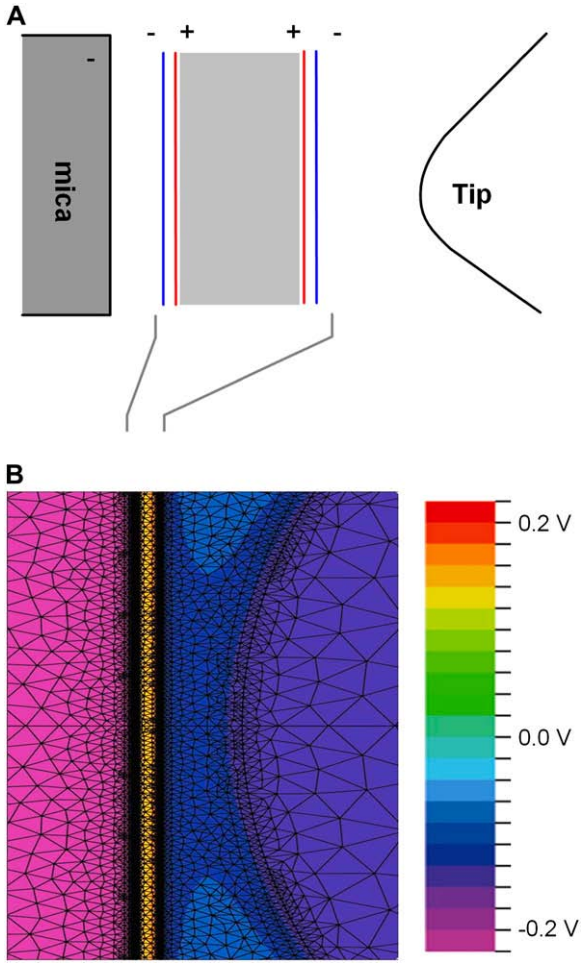

FIGURE 3 Numerical simulation of the tip-dipole interaction. (*A*) A schematic of the tip-sample region, illustrating the planes of charge used to model the molecular membrane dipoles and the hydrophobic region of the lipid bilayer (*shaded*). (*B*) A portion of a mesh from the numerical simulations of the tip-dipole interaction.

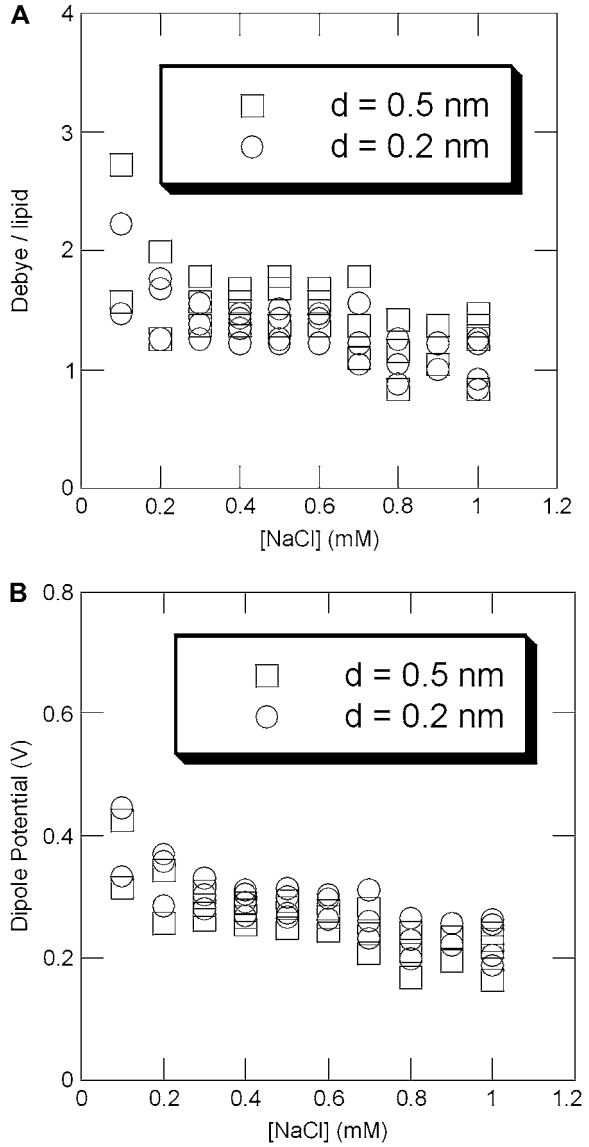

FIGURE 4 The dipole density (*A*) and dipole potential (*B*) of a supported DOPC membrane as determined by analysis of electrostatic interactions measured with the AFM. The results are plotted for analysis with two different charge plane separations according to the schematic in Fig. 3 *A*.

measurements over an identical reference sample as described previously (13). An example of the simulation mesh is shown in Fig. 3 *B*. The simulations were run as a function of tip-sample separation, and the resulting surface potentials were converted to forces using the total stress tensor, which includes both an entropic and a Maxwell electrostatic term (13). The charge densities on these planes were then manually adjusted to fit the experimental force curves by minimizing the sum square error between the simulated and experimental force curves. The result of the numerical dipole analysis is displayed in Fig. 4. The 2 Å and 5 Å charge plane separations yield similar results: dipole densities of ~1.5 Debye per lipid, and dipole potentials ranging from 200 mV to 400 mV with a slight dependence on electrolyte concentration. Note that the different charge plane separations in the numerical simulation result in similar dipole densities. Since the AFM tip only experiences the external field at a large distance from the membrane (>10 nm), one would expect the result to be independent of molecular details. Therefore, the lack of dependence of our measurements on simulated charge plane separation supports our application of a continuum model to analyze this data even though it was recorded near the molecular scale.

The AFM analysis of the dipole potential yields results similar to those from ion transport measurements through lipid bilayers. However, the AFM method is quite novel in several respects. First, the measurements are highly noninvasive. The force curves are recorded at a tip-sample separation of >10 nm, which is ~1 Debye screening length for 1-mM electrolyte. This is much less invasive than hydrophobic ion transport, monolayer formation, or the insertion of molecular probes. Second, the AFM measurements are accurate and quantitative in the sense that the model used to interpret the data is quite straightforward, requiring only the Poisson-Boltzmann equation and the classical stress tensor with no free parameters. Although the charge density and separation of the dipolar planes can be independently varied, Fig. 4 demonstrates that the result depends only on their product, the dipole density. Third, the AFM measurements can be made with nanometer-scale lateral resolution. Fig. 5 presents AFM topographic and electrostatic maps of lipid membranes containing DOPC, sphingomyelin (SM), and cholesterol that form liquid-ordered microdomains known as lipid rafts (23). These domains are models of those thought to

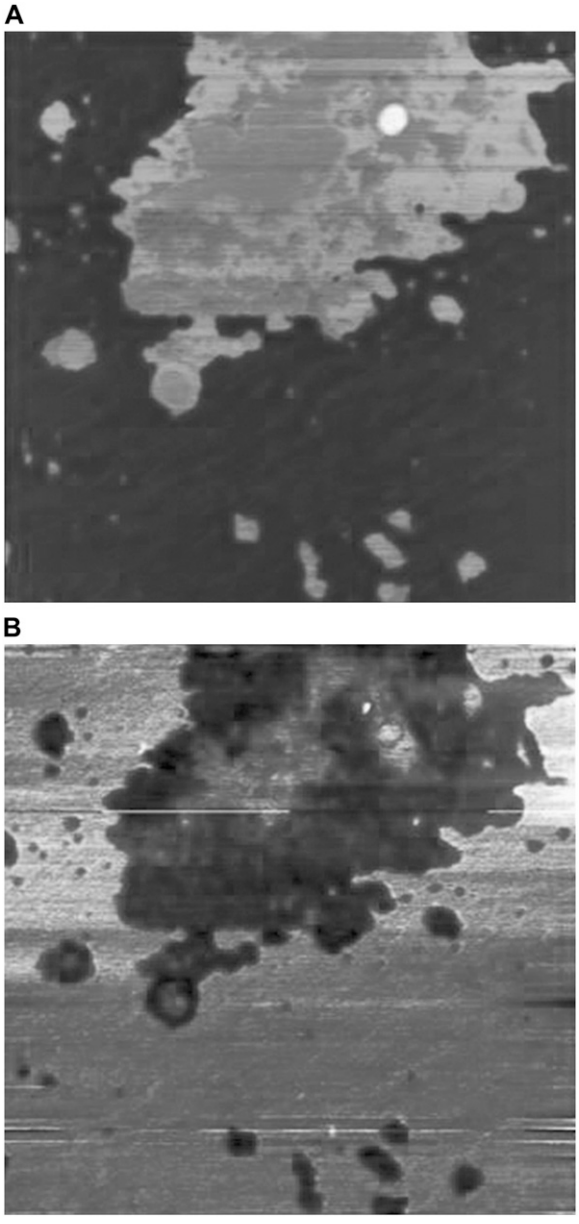

FIGURE 5 The topography (*A*) and surface charge map (*B*) of a DOPC/SM/cholesterol supported membrane exhibiting lipid rafts recorded with the AFM. Each image is 5 × 5 μm.

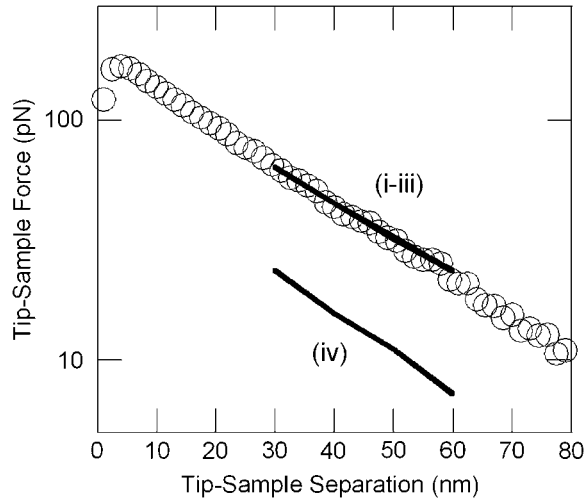

FIGURE 6 The effect of mica surface charge on the dipole simulations. Force data (*circles*) are plotted with results from the dipole model (*lines*) with an optimized dipole density of 1.5 Debye/lipid and mica surface charge of −0.01 C/m^2 (*i*), 1.5 Debye/lipid and 0.0 C/m^2 (*ii*), and 1.5 Debye/lipid and +0.01 C/m^2 (*iii*). The results of these three simulations are very similar. A fourth simulation is displayed for 0.0 Debye/lipid and −0.01 C/m^2 (*iv*).

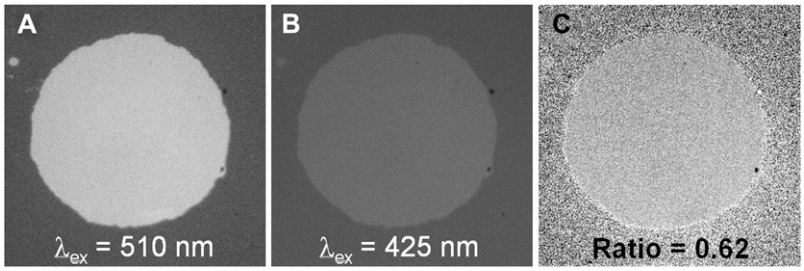

FIGURE 7 Ratiometric fluorescence imaging of a supported DOPC lipid membrane with Di-8-ANEPPS. Fluorescence images were bandpass-filtered at 675 nm with excitation wavelengths of 510 nm (*A*) and 425 nm (*B*). The ratio of the images (425 nm/510 nm) is displayed in panel *C*. The average ratio value is 0.62.

exist in natural biomembranes and may have biological significance. The topographic image reveals the liquid-ordered raft phase based on increased height (24). The electrostatic map, taken by a method we developed previously (14), clearly shows a variation in effective surface charge density between the liquid-ordered and liquid-disordered regions. Since the DOPC and SM are both zwitterionic, we can interpret the contrast as a variation in the membrane dipole density.

Rather than the dipole potential, the data of Fig. 1 *B* could be the result of a simple repulsive interaction between the negatively charged tip and negatively charged mica beneath the lipid membrane. Two lines of evidence suggest that this is not the case. First, a typical value of -0.01 C/m^2 for the mica charge density is included in all of the dipole simulations for data analysis (22). To confirm that the mica charge is not responsible for the repulsive force, the data were simulated with negative, positive, and zero mica charge, and it had no effect on the result (Fig. 6). Furthermore, when the mica was given a negative charge and the dipole density was removed, the simulation predicted a significantly underestimated force. Therefore, to the extent that the simulation correctly describes the interaction, the observed forces are dominated by the dipole potential rather than the mica surface charge. Second, the topography and charge map displayed in Fig. 5 reveal a strong variation in electrostatics corresponding to a slight change in membrane thickness between the liquid-ordered and liquid-disordered regions. If the electrostatic interaction were due to the mica charge, one would not expect a strong variation since the two lipid regions are of similar thickness and would screen the mica by a similar amount. However, the difference between the liquid-ordered and liquid-disordered lipid regions does have a strong influence on the molecular structure at the interfacial planes where the dipole moment is defined.

The dipole potential is expected to influence the biological function of membranes, since the large associated fields at the interfacial membrane planes could affect protein conformation (25). There have been occasional reports on such correlations, including dipole potential effects on signal peptide conformation (26), ion channel activity (27–29), enzymatic activity (30), membrane fusion (31), and receptor-ligand interactions on cells (32). However, no direct mechanistic explanations or definitive conclusions have been drawn from these studies, due to the imprecise knowledge of the dipole potential, and to the fact that the dyes and sterols used to measure and manipulate the dipole potential could have specific interactions with membrane proteins. The AFM technique described here can greatly reduce these limitations. Furthermore, the AFM technique can be used to calibrate precisely the response of voltage sensitive dyes to the dipole potential. This would be especially useful in cellular studies that require rapid measurements on unsupported membranes. To demonstrate this possibility, mica-supported zwitterionic membranes were prepared with 1:600 di-8-ANEPPS:DOPC and imaged by fluorescence microscopy at two excitation wavelengths (Fig. 7). The ratiometric emission image at 675 nm, which minimizes the effects of membrane fluidity on the measurement (33), reveals a constant value of 0.62 over the lipids, which corresponds to the ratio reported for unsupported membranes (10). This measurement represents the first step in a precise calibration of voltage sensitive dyes to the dipole potential.

The biological function of the interfacial field associated with the dipole potential is one of many questions in the rapidly emerging view that the lipid environment contributes significantly to membrane function through its effect on membrane proteins. This effect can include such phenomena as local sequestration of signaling factors to the membrane and specific lipid-protein interactions. Many studies along these lines have focused on mechanical effects of the lipid composition, such as membrane thinning and microviscosity, although some have considered electrostatic effects (2,34). The AFM techniques described here will be highly beneficial to these studies because the AFM can simultaneously perform quantitative analysis of the interfacial electrostatics and measurement of the membrane thickness and stiffness. Thus, the AFM can be used to distinguish electrostatic and mechanical effects on membrane function.

The authors gratefully acknowledge funding from National Science Foundation grant Nos. CHE-0517937, EEC-018007, and EEC-0647452.

REFERENCES

1. MacKinnon, R. 2004. Voltage sensor meets lipid membrane. *Science*. 306:1304–1305.
2. McLaughlin, S., and D. Murray. 2005. Plasma membrane phosphoinositide organization by protein electrostatics. *Nature*. 438:605–611.
3. Clarke, R. J. 2001. The dipole potential of phospholipid membranes and methods for its detection. *Adv. Colloid Interface Sci.* 89:263–281.

4. Liberman, Y. A., and V. P. Topaly. 1969. Permeability of bimolecular phospholipid membranes for fat-soluble ions. *Biophysics*. 14:477–487.
5. Haydon, D. A., and V. B. Myers. 1973. Surface charge, surface dipoles and membrane conductance. *Biochim. Biophys. Acta*. 307:429–443.
6. Schamberger, J., and R. J. Clarke. 2002. Hydrophobic ion hydration and the magnitude of the dipole potential. *Biophys. J*. 82:3081–3088.
7. Franklin, J. C., and D. S. Cafiso. 1993. Internal electrostatic potentials in bilayers—measuring and controlling dipole potentials in lipid vesicles. *Biophys. J*. 65:289–299.
8. Brockman, H. 1994. Dipole potential of lipid membranes. *Chem. Phys. Lipids*. 73:57–79.
9. Berkowitz, M. L., D. L. Bostick, and S. Pandit. 2006. Aqueous solutions next to phospholipid membrane surfaces: insights from simulations. *Chem. Rev*. 106:1527–1539.
10. Gross, E., R. S. Bedlack, and L. M. Loew. 1994. Dual-wavelength ratiometric fluorescence measurement of the membrane dipole potential. *Biophys. J*. 67:208–216.
11. Klymchenko, A. S., G. Duportail, Y. Mely, and A. P. Demchenko. 2003. Ultrasensitive two-color fluorescence probes for dipole potential in phospholipid membranes. *Proc. Natl. Acad. Sci. USA*. 100:11219–11224.
12. Wang, L. G., P. S. Bose, and F. J. Sigworth. 2006. Using cryo-EM to measure the dipole potential of a lipid membrane. *Proc. Natl. Acad. Sci. USA*. 103:18528–18533.
13. Yang, Y., K. M. Mayer, and J. H. Hafner. 2007. Quantitative membrane electrostatics with the atomic force microscope. *Biophys. J*. 92: 1966–1974.
14. Johnson, A. S., C. L. Nehl, M. G. Mason, and J. H. Hafner. 2003. Fluid electric force microscopy for charge density mapping in biological systems. *Langmuir*. 19:10007–10010.
15. Cleveland, J. P., S. Manne, D. Bocek, and P. K. Hansma. 1993. A nondestructive method for determining the spring constant of cantilevers for scanning force microscopy. *Rev. Sci. Instrum*. 64:403–405.
16. Hillier, A. C., S. Kim, and A. J. Bard. 1996. Measurement of double-layer forces at the electrode/electrolyte interface using the atomic force microscope: potential and anion dependent interactions. *J. Phys. Chem*. 100:18808–18817.
17. Israelachvili, J. 1991. Intermolecular and Surface Forces. Academic Press, San Diego, CA.
18. Eisenberg, M., T. Gresalfi, T. Riccio, and S. McLaughlin. 1979. Adsorption of monovalent cations to bilayer membranes containing negative phospholipids. *Biochemistry*. 18:5213–5223.
19. Cevc, G. 1990. Membrane electrostatics. *Biochim. Biophys. Acta*. 1031: 311–382.
20. Pandit, S. A., D. Bostick, and M. L. Berkowitz. 2003. Molecular dynamics simulation of a dipalmitoylphosphatidylcholine bilayer with NaCl. *Biophys. J*. 84:3743–3750.
21. Belaya, M., V. Levadny, and D. A. Pink. 1994. Electric double-layer near soft permeable interfaces.1. Local electrostatics. *Langmuir*. 10: 2010–2014.
22. Pashley, R. M. 1981. DLVO and hydration forces between mica surfaces in Li^+, Na^+, K^+, and Cs^+ electrolyte-solutions—a correlation of double-layer and hydration forces with surface cation-exchange properties. *J. Colloid Interface Sci*. 83:531–546.
23. Edidin, M. 2003. The state of lipid rafts: from model membranes to cells. *Annu. Rev. Biophys. Biomol. Struct*. 32:257–283.
24. Geisse, N. A., T. L. Cover, R. M. Henderson, and J. M. Edwardson. 2004. Targeting of *Helicobacter pylori* vacuolating toxin to lipid raft membrane domains analyzed by atomic force microscopy. *Biochem. J*. 381:911–917.
25. O'Shea, P. 2003. Intermolecular interactions with/within cell membranes and the trinity of membrane potentials: kinetics and imaging. *Biochem. Soc. Trans*. 31:990–996.
26. Cladera, J., and P. O'Shea. 1998. Intramembrane molecular dipoles affect the membrane insertion and folding of a model amphiphilic peptide. *Biophys. J*. 74:2434–2442.
27. Ostroumova, O. S., Y. A. Kaulin, P. A. Gurnev, and L. V. Schagina. 2007. Effect of agents modifying the membrane dipole potential on properties of syringomycin E channels. *Langmuir*. 23:6889–6892.
28. Duffin, R. L., M. P. Garrett, K. B. Flake, J. D. Durrant, and D. D. Busath. 2003. Modulation of lipid bilayer interfacial dipole potential by phloretin, RH421, and 6-ketocholestanol as probed by gramicidin channel conductance. *Langmuir*. 19:3561−3563.
29. Starke-Peterkovic, T., N. Turner, P. L. Else, and R. J. Clarke. 2005. Electric field strength of membrane lipids from vertebrate species: membrane lipid composition and Na^+-K^+-ATPase molecular activity. *Am. J. Physiol. Regul. Integr. Comp. Physiol*. 288:R663–R670.
30. Maggio, B. 1999. Modulation of phospholipase A_2 by electrostatic fields and dipole potential of glycosphingolipids in monolayers. *J. Lipid Res*. 40:930–939.
31. Cladera, J., I. Martin, J. M. Ruysschaert, and P. O'Shea. 1999. Characterization of the sequence of interactions of the fusion domain of the simian immunodeficiency virus with membranes—role of the membrane dipole potential. *J. Biol. Chem*. 274:29951–29959.
32. Asawakarn, T., J. Cladera, and P. O'Shea. 2001. Effects of the membrane dipole potential on the interaction of saquinavir with phospholipid membranes and plasma membrane receptors of CACO-2 cells. *J. Biol. Chem*. 276:38457–38463.
33. Clarke, R. J., and D. J. Kane. 1997. Optical detection of membrane dipole potential: avoidance of fluidity and dye-induced effects. *Biochim. Biophys. Acta Biomembr*. 1323:223–239.
34. Schmidt, D., Q. X. Jiang, and R. MacKinnon. 2006. Phospholipids and the origin of cationic gating charges in voltage sensors. *Nature*. 444: 775–779.